IEEE Access
Multidisciplinary | Rapid Review | Open Access Journal

Received February 26, 2019, accepted March 16, 2019, date of publication March 20, 2019, date of current version April 8, 2019.

Digital Object Identifier 10.1109/ACCESS.2019.2906329

Shunt Isolated Active Power Filter With Common DC Link Integrating Braking Energy Recovery in Urban Rail Transit

HAO LIU[1, 2], (Student Member, IEEE), CHI LI[1], (Member, IEEE), ZEDONG ZHENG[1], (Member, IEEE), JIYE LIU[1], (Student Member, IEEE), AND YONGDONG LI[1], (Member, IEEE)

[1]State Key Laboratory of Power System, Department of Electrical Engineering, Tsinghua University, Beijing 100084, China
[2]National Key Laboratory of Power System, Shenzhen Graduate School at Shenzhen, Tsinghua University, Shenzhen 518055, China

Corresponding author: Zedong Zheng (zzd@mail.tsinghua.edu.cn)

This work was supported in part by the National Natural Science Foundation of China under Grant 51777111, and in part by the Natural Science Foundation of Beijing Municipality under Grant 3161001.

ABSTRACT In urban rail transit, there is a large number of harmonics brought by diode rectifiers, and shunt active power filters (APFs) are an effective method of harmonics rejection. Traditional shunt APFs work with a dedicated DC link leading to complexity, while those with a common DC bus but using non-isolated topologies bring serious problems of zero-sequence circulating current (ZSCC), which introduce losses and provoke poor quality. Consequently, this paper first analyzes the limitations of traditional non-isolated APFs on modulation radio. Based on the analysis, this paper put forward a novel isolated APF with a common DC link based on existing diode rectifiers in urban rail transit, which realizes braking energy recovery as an additional function. To this end, harmonics brought by diode rectifiers are reduced while rejecting ZSCC. Meanwhile, braking energy can feedback to the city grid with lower harmonics. Finally, simulation and experiment using a 1-kW prototype converter verify the feasibility and validity of the proposed converter on harmonics suppression and braking energy recovery.

INDEX TERMS Active power filter (APF), LLC series resonant converter, soft switching, braking energy recovery, zero sequence circulating current (ZSCC).

I. INTRODUCTION

Harmonics pollution generated by non-linear loads results in poor quality of city grids so that IEEE standards are issued [1]. With the expanding scale of urban rail transit, impact of harmonics gets more attention considering both the grid and the equipment. In traction grids and distribution grids of urban rail transit, 3-phase diode rectifiers are widely applied in driving motors or equipment such as lighting, ventilation, elevators and so on, which generate harmonics inevitably (especially 5^{th} or 7^{th} harmonics) causing distortion of voltage and current waveforms [2], [3]. High-frequency harmonics will provoke electromagnetic disturbances while low-frequency components also need reactive elements to compensate. What is worse, harmonic contents bring additional losses (iron losses and copper losses), vibrations in motors and resonances in local grids, decrease in insulation property and equipment life [4].

In order to eliminate the harmonics in urban rail transit, passive power filters (PPFs) based on LC elements can be applied. But the characteristics of filtering are sensitive to parameters and dynamic responses of filtering cannot be realized [5]. In hence, multi-pulse rectifiers and APFs are two effective methods [6], [7]. Compared to multi-pulse rectifiers, shunt APFs or series APFs are flexible and can release the applications of line-frequency transformers which take up a large volume [8]. Series APFs are used for voltage harmonic sources and shunt APFs are usually used to compensate current harmonic sources such as 3-phase diode rectifiers with RL loads, which are mature and more widely applied. They inject compensating currents to keep sinusoidal source current balanced. However, drawbacks of traditional APFs

The associate editor coordinating the review of this manuscript and approving it for publication was Yuh-Shyan Hwang.

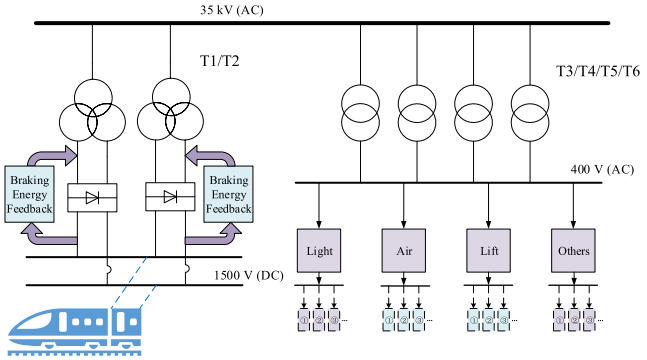

FIGURE 1. AC distribution architecture of the urban rail transit.

are of lower efficiency and high complexity, especially with a dedicated DC link for shunt APFs, which is not preferred in urban trail transit. Diode rectifiers are widely implemented to power the trains, as shown in Fig. 1, and existing DC links formed by diode rectifiers can be utilized by shunt APFs. Thus, a shunt APF for single-phase and 3-phase was studied, in which 3-phase inverter has a common DC link with diode rectifiers [9], [10]. This non-isolated APF leads to potential paths of zero sequence circulating current (ZSCC) and even considering optimized modulation methods, ZSCC suppression can only be achieved at the sacrifice of modulation radio and DC voltage utilization, which is theoretically analyzed in section III. In hence, electrical isolation is necessary in this kind of topologies of shunt APFs.

Traditionally, line-frequency transformers can achieve galvanic isolation, power conversion and match voltage between two sides. But bulky, heavy and noisy line-frequency transformers will set a limit on its application [11], [12]. Nowadays, topologies of converters based on high-frequency power electronics transformers (HFPET) are put forward so that the efficiency increases while the volume sharply decreases. For the topologies of isolated DC/DC converters, a dual-active-bridge (DAB) is often used in battery energy storage systems. However, soft-switching range decreases under light load [13], [14]. It is inevitable that modulation strategies for extending soft-switching range are complex with both online and offline calculation. In hence, to address these problems, LLC series resonant converter can both achieve zero-voltage-switching (ZVS) for primary side switches and zero-current-switching (ZCS) for secondary side diode rectifiers at most load conditions [15]–[17].

In addition, a shunt isolated APF with a common DC link can also serve in braking energy recovery as an auxiliary function. For urban rail transit, braking energy recovery has earned much attention recently because of its contribution to reducing a large waste of energy and smoothing fluctuation of traction grids. Because of the application of diode rectifiers, redundant regenerating energy cannot inject into medium-voltage grids [18]–[22]. As for 60% $\sim$ 70% of braking energy has been absorbed between processes of braking and starting, about 200 kW$\sim$300 kW needs a path for energy dissipation or recovery [23]. Among the three mainstream

TABLE 1. Comparison among 3 types of solutions on braking energy recovery and APF.

	Replacing Completely	Replacing Partly	Placing Additionally
Volume	Small	Small	Medium
Cost	High	Low	Medium
Traction Capacity	Low	Medium	High
Recovery Capacity	Medium	Low	Low
Harmonics	Low	Medium	Low
Reliability	Low	Medium	High

methods – integrating braking resistors, energy storage systems and braking energy recovery, resistors will generate heat with extra burden for ventilating systems at stations and it is expensive to install and maintain energy storage systems. Thus, braking energy feedback to city grids is considered as an effective way, which can be realized by a shunt isolated APF.

To suppress the harmonics and realize braking energy recovery, there are mainly three types of solutions including 1) replacing all diode rectifiers with bi-directional converters, 2) partly replacing diodes and 3) placing additional converters. Comparison among 3 types of solutions is shown in table 1 based on volume, cost, capacity of traction and recovery, harmonics and reliability [24]. A PWM rectifier is a typical approach in solution 1 considering of its characteristics of high power factor, low harmonics and inherent power recuperation capability [25], [26].

Compared with diode rectifiers, PWM rectifiers have four times higher losses with related expenses on the cooling system and 2.5 times higher power semiconductor [27].

Accompanied by the development and cost reduction of large power devices, PWM rectifiers may be the best system solution for new traction substations eventually. However, when modifying all existing substations with PWM rectifiers, all diodes rectifiers and the transformer have to be replaced which brings a huge cost. Therefore, an alternative braking energy recovery solution with the minimal changes should be taken in the existing installations [28], [29].

This paper is organized as follows: first in section II, architecture of urban rail transit, harmonics pollution brought by diode rectifiers and braking energy recovery are analyzed. Second, the ZSCC paths existing in a non-isolated APF sharing a common link with a diode rectifier is analyzed and calculated in section III. In section IV, the shunt isolated APF topology integrated with the braking energy recovery function is presented, together with operating mode analysis and closed-loop control strategy. Finally, the system model, topology and control strategy are verified via simulation and experiment in section V and VI.

II. ARCHITECTURE OF URBAN RAIL TRANSIT AND ANALYSIS ON BRAKING ENERGY RECOVERY

A. ARCHITECTURE OF URBAN RAIL TRANSIT

Presently, line-frequency transformers are applied in traction grids transforming AC 35 kV (10 kV) to AC 1,180 V and

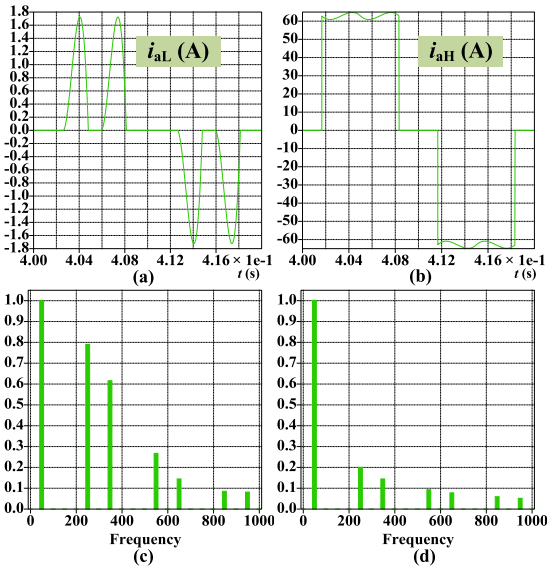

FIGURE 2. Harmonics generated by diode rectifiers (a) (c) are characteristic of light load and (b) (d) are of heavy load.

diode rectifiers transform power from AC to DC 1,500 V (750 V). Besides, an AC distribution grid, in which light, air, lift and other loads are connected to, is separated from the traction grid. The architecture of the system is shown in Fig. 1. Isolated DC/DC converters are the key technology in the DC distribution or the traction grids to realize power transfer between loads or sources to DC grids [30]. In order to recover braking energy, adding a shunt braking energy recovery is more practicable than replacing the rectifiers directly, considering the reliability and cost.

In the urban rail transit, diode rectifiers have brought harmonics, which is the largest harmonics sources due to their non-linear characteristics, leading to voltage distortions of the urban rail transit [31], [32]. Under the condition of light load and heavy load, phase current of diode rectifiers is in intermittent or continuous operating mode respectively. The AC currents of diode rectifiers are shown in Fig. 2 and Fast Fourier Transform (FFT) analysis is done under load factor of 1% and 90% respectively, in which i_{aL} (A) and i_{aH} (A) are current of light and heavy loads respectively. THD (total harmonic distortion) is up to 160% for light load and 45% for heavy load respectively. The results of FFT analysis show that 5, 7, 11, 13 . . .(6n ±1) order harmonics have taken up a mainly part.

B. ANALYSIS ON BRAKING ENERGY RECOVERY

During the process of braking, force and movement equations of trains are listed as (1), (2), (3) where braking force of train F_B (N), friction of operating F_o (N), velocity of train v (km/h), initial velocity of trains v_1 (km/h) and braking distance s (m) are used. F_o (N) can be divided to basic friction F_f (N) and additional friction F_a (N). F_f represents the movement

TABLE 2. Parameters of a type in Guangzhou metro of china.

Symbol	Quantity	Parameters
P_B	Nominal power of each asynchronous machine	190 kW
m	Mass of the train	40 t
a		1.97
b	Force parameter of train	0.015
c		0.000156

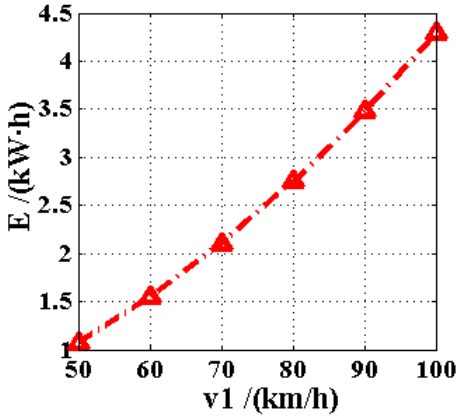

FIGURE 3. Curve of braking energy E(kW·h) and v_1(km/h) during braking process of the train.

characteristic of the train. As F_a is raised by arc of the road, air friction and drag between wheels and rail which can be ignored. In hence, F_o can be calculated by the equation (1) according to the empirical formula, where a, b and c are decided by parameters of the train. Braking energy E (J) can be calculated through equation (2), where m (kg) is the mass of the train. The parameters of a certain train are listed in table 2, where P_B(kW) is the nominal power of each asynchronous machine and the traction power of train is around 3,000 kW. Calculation results are shown in Fig. 3 including relationships between E and v_1.

$$F_o \approx F_f = a + bv + cv^2 \tag{1}$$

$$E = \frac{mv^2}{2} - F_o s \tag{2}$$

$$m\frac{d^2s}{dt^2} = -F_B - F_o \tag{3}$$

Based on the calculation, for a train at the speed of 70 km/h, it will generate 2.1 kW·h energy during a single braking within 10 s, with an average power of braking of 756 kW. The daily operating time of the railway line is 17 hours and braking times of the trains in a station is 60 within an hour. Considering the price of electricity is $ 0.073 / (kW·h), total profits generated by braking recycling in one year is about $ 26,180.

The voltage of traction grid increases when the train brakes while the voltage keeps steady during the starting and running process of trains. In a urban rail transit with multiple trains, about 60% ∼ 70% of braking energy can be absorbed in the

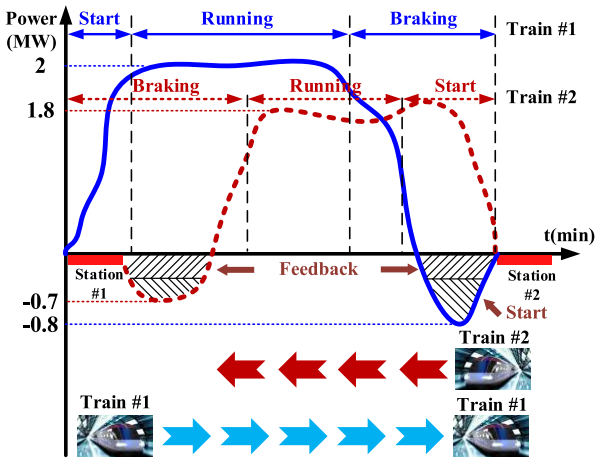

FIGURE 4. Power curves at various periods in the system of multiple trains.

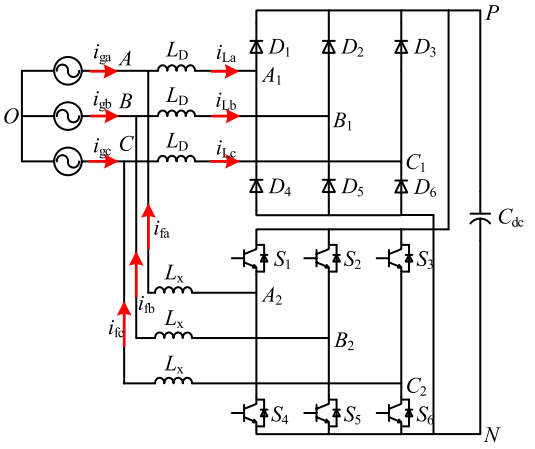

FIGURE 5. Shunt topology of diode rectifier and non-isolated inverter.

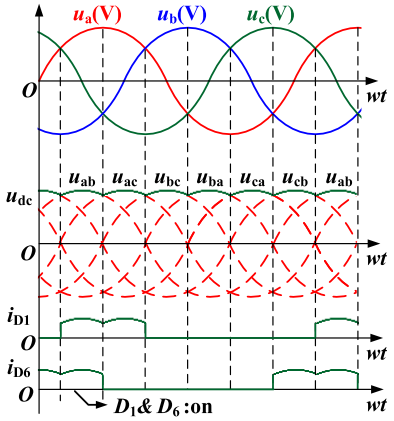

FIGURE 6. Voltage waves and switching states of diode rectifiers.

starting process of another train, which is shown in Fig. 4. Except for this part of braking energy, the rest 200 kW of energy can be injected to city grid by feedback devices. In hence, smaller capacity of braking energy recovery equipment can be set compared to traction power [33].

III. ANALYSIS OF ZERO SEQUENCE CIRCULATING CURRENT

In the urban rail transit shown in Fig. 1, harmonics need to be suppressed by applying shunt APFs. Reference [10] has shown that existing DC link formed by diode rectifiers can be utilized by shunt APFs. In this way, a 3-phase inverter can have a common DC link with the diode rectifier, which forms a shunt non-isolated topology. Limitations of this shunt non-isolated topology including losses and low modulation radio are analyzed specifically in this section.

In urban rail transit, diode rectifiers usually provoke high harmonics and shunt non-isolated APF converter has been applied to suppress it. In addition, APFs with common DC link have also been developed in order to release a dedicated capacitor, topology of which is shown Fig. 5, in which output current of inverter i_{fa} (A), i_{fb} (A),i_{fc} (A), current of diode rectifier i_{La} (A), i_{Lb} (A),i_{Lc} (A), and grid current i_{ga} (A), i_{gb} (A)i_{gc} (A) are shown. In shunt non-isolated topology, circulating currents may increase losses, decreasing efficiency and bringing distortion of current and voltage [34]. On the side of grid, equation (4) (5) can be obtained due to symmetry of the 3-phase city grid. As the existence of i_{La} (A), i_{Lb} (A),i_{Lc} (A), ZSCC i_{ZSCC} (A) can be defined as equation (6) and be used to calculate, in which i_{fa} (A), i_{fb} (A), i_{fc} (A) are the output currents of the 3-phase inverter.

$$i_{ga} + i_{gb} + i_{gc} = 0 \tag{4}$$

$$i_{fa} + i_{fb} + i_{fc} = i_{La} + i_{Lb} + i_{Lc} \tag{5}$$

$$i_{ZSCC} = i_{fa} + i_{fb} + i_{fc} = \sum_{x=a,b,c} i_{Lx} \tag{6}$$

During the operating process of the train, diode rectifiers transform power from AC to DC to power the train. APFs are operating to suppress harmonics carrying power from DC link to AC. So the loop of ZCSS is formed between 3-phsae inverter and diode rectifiers. Operating waves of diode rectifiers in one period is shown in Fig. 6. One sixth of the period is considered specifically as below in which D_1, D_6 are conducting. For example, when S_1, S_2, S_6 are conducting and S_3, S_4, S_5 are switched off, the topologies and paths of ZSCC are shown in Fig. 7. The loops of the ZSCC are listed as follows (Loop 1 & Loop 2).

Loop 1: A_2-L_{a2}-A-L_D-A_1-D_1-P-S_1-A_2

Loop 2: C_2-S_2-N-D_6-C_1-L_D-C-L_{c2}-C_2

Let us use switching functions S_a, S_b, S_c to represent operating states of switches in phase A, B and C, definitions of which are shown in equation (7). For the PWM control of the 3-phase inverter, all the switching states are shown in table 3, in which ZSCC loops of different states of the inverter are shown. When all the six switches are switched off, 3-phase inverter will act as diode rectifiers so that whole system can be recognized as two shunt diode rectifiers.

$$S_{a(b,c)} = \begin{cases} 1, & \text{Upper arm of phase A(B, C) is on} \\ 0, & \text{Lower arm of phase A(B, C) is on} \end{cases} \tag{7}$$

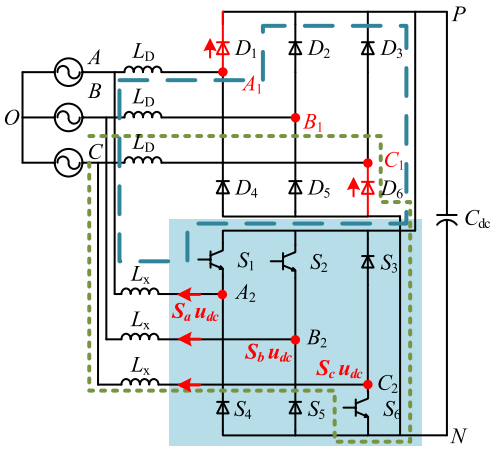

FIGURE 7. Operating mode of shunt topology (on-state: S_1, S_2, S_6; off-state: S_3, S_4, S_5).

TABLE 3. ZSCC loops on condition of different switching states of 3-phase inverter.

No.	S_a	S_b	S_c	ZSCC Loops
1	0	0	0	Loop 2
2	0	0	1	No ZSCC
3	0	1	0	Loop 2
4	0	1	1	No ZSCC
5	1	0	0	Loop 1; Loop 2
6	1	0	1	Loop 1
7	1	1	0	Loop 1; Loop 2
8	1	1	1	Loop 1

The equivalent circuit of the ZSCC based on Loop 1 and Loop 2 are shown in Fig. 8. L_x are inductances of the 3-phase inverter and L_D are the relatively small stray inductance of the diode rectifier. Because of circuit symmetry, L_x are nearly equal and the sum of 3-phase voltage is equal to zero. Besides, u_{dc}(V) and u_x (V) are the voltage of DC bus and the phase-voltage of phase x.

Firstly, let us consider the ZCSS crossing D_1. No. 6 and 8 states shown in table 3 only have Loop 1. According to the equivalent circuit shown in Fig. 8, equation (8) and (9) can be gotten, where u_{ON}(V) means the voltage between O and N. By the definition shown in equation (6) and (10), u_{ON}(V) and di_{ZSCC}/dt are gotten as equation (11) and (12) respectively.

$$\begin{cases} S_a \times u_{dc} = L_x \dfrac{di_{fa}}{dt} + u_a + u_{ON} \\ S_b \times u_{dc} = L_x \dfrac{di_{fb}}{dt} + u_b + u_{ON}, \quad k = \dfrac{L_x}{L_D} \\ S_c \times u_{dc} = L_x \dfrac{di_{fc}}{dt} + u_c + u_{ON} \end{cases} \tag{8}$$

$$u_{dc} = -L_D \frac{di_{La}}{dt} + u_a + u_{ON} \tag{9}$$

$$i_{ZSCC} - i_{La} = 0 \tag{10}$$

$$u_{ON} = \frac{(S_a + S_b + S_c) \times u_{dc} + k u_{dc} - k u_a}{k+3} \tag{11}$$

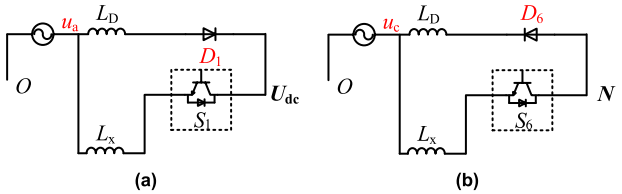

FIGURE 8. Equivalent circuit of ZSCC (a) ZSCC crossing D_1 (b) ZSCC crossing D_6.

$$\frac{di_{ZSCC}}{dt} = \frac{(S_a + S_b + S_c - 3) \times u_{dc} + 3 \times u_a}{(k+3)L_D} \tag{12}$$

Similarly, No. 1 and 3 states shown in table 3 only have Loop 2. i_{ZSCC} can be recognized as equation (13). Calculations on u_{ON}(V) and di_{ZSCC}/dt are shown as equations (14), (15) and (16).

$$i_{ZSCC} - i_{Lc} = 0 \tag{13}$$

$$u_{ON} = L_D \frac{di_{Lc}}{dt} - u_c \tag{14}$$

$$u_{ON} = \frac{(S_a + S_b + S_c) \times u_{dc} - k u_c}{k+3} \tag{15}$$

$$\frac{di_{ZSCC}}{dt} = \frac{(S_a + S_b + S_c) \times u_{dc} + 3 \times u_c}{(k+3)L_D} \tag{16}$$

In addition, No. 5 and 7 states shown in table 3 have both Loop 1 and Loop 2. i_{ZSCC} can be recognized as equation (17). Both calculations of Loop 1 and Loop 2 are done respectively.

$$i_{ZSCC} - i_{La} - i_{Lc} = 0 \tag{17}$$

Calculations on Loop 1 for states 5 and 7 are gotten as equation (18) and (19).

$$u_{ON} = \frac{(S_a + S_b + S_c + k)u_{dc} - k u_a}{k+3} - \frac{k L_D}{k+3} \times \frac{di_{Lc}}{dt} \tag{18}$$

$$\frac{di_{\mathrm{La}}}{dt} + \frac{k}{k+3}\frac{di_{\mathrm{Lc}}}{dt} = \frac{(S_a + S_b + S_c - 3)u_{dc} + 3u_a}{(k+3)L_D} \tag{19}$$

0

Calculations on Loop 2 for states 5 and 7 are gotten as equation (20) and (21). In hence, di_{ZSCC}/dt are shown as equation (22).

$$u_{ON} = \frac{(S_a + S_b + S_c)u_{dc} - k u_c}{k+3} - \frac{k L_D}{k+3} \times \frac{di_{La}}{dt} \tag{20}$$

$$\frac{di_{\mathrm{Lc}}}{dt} + \frac{k}{k+3}\frac{di_{\mathrm{La}}}{dt} = \frac{(S_a + S_b + S_c)u_{dc} + 3u_c}{(k+3)L_D} \tag{21}$$

$$\frac{di_{ZSCC}}{dt} = \frac{di_{\mathrm{La}}}{dt} + \frac{di_{\mathrm{Lc}}}{dt} = \frac{[2(S_a + S_b + S_c) - 3]u_{dc} + 3u_a + 3u_c}{(2k+3)L_D} \tag{22}$$

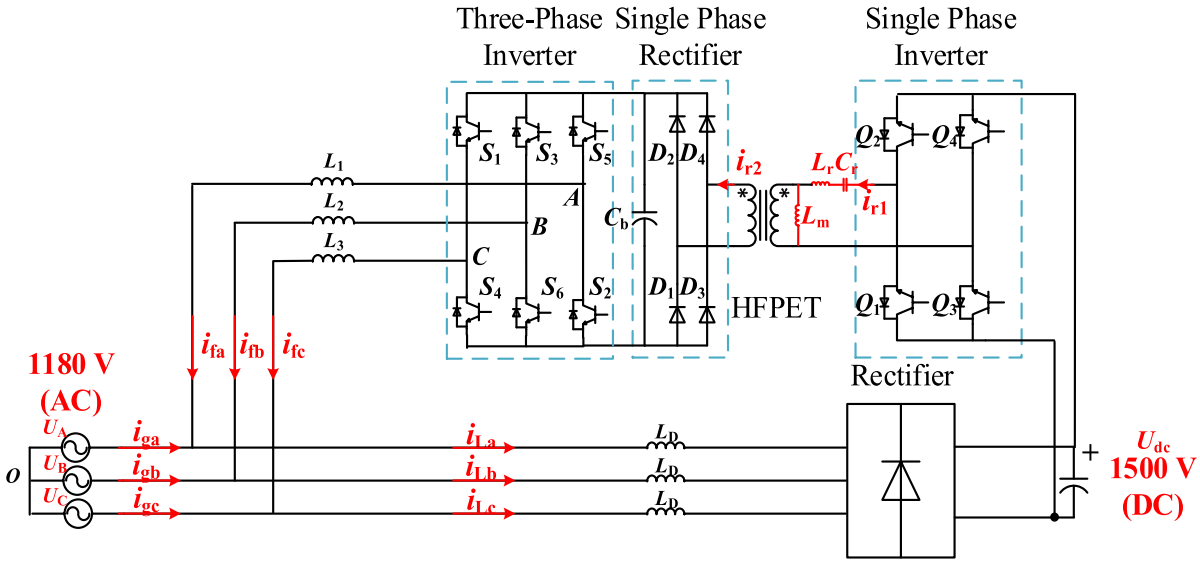

FIGURE 9. Topology of the shunt isolated APF with common DC link integrating braking energy recovery based on HFPET and LLC converter.

According to the calculations based on three conditions shown above, results can be expanded to other operating conditions of diode rectifiers based on relationships among 3-phase voltage u_a(V), u_b(V), u_c(V). By equation (23) and (24) in which M, m mean the phase, calculation results in whole period of diode rectifiers are generalized as equation (25). When 3-phase inverter is operating under $S_M = 0$ & $S_m = 1$, ZSCC does not exist because of no circulating paths.

$$u_M = Max\{u_a, u_b, u_c\};\ u_m = Min\{u_a, u_b, u_c\} \tag{23}$$

$$U = 3S_M u_M + 3(1 - S_m)u_m \tag{24}$$

$$\frac{di_{ZSCC}}{dt} = \begin{cases} \dfrac{(S_a + S_b + S_c - 3) \times u_{dc} + U}{(k+3)L_D}; \\ \qquad S_M = 1,\ S_m = 1 \\ \dfrac{(S_a + S_b + S_c) \times u_{dc} + U}{(k+3)L_D}; \\ \qquad S_M = 0,\ S_m = 0 \\ \dfrac{[2(S_a + S_b + S_c) - 3]u_{dc} + U}{(2k+3)L_D}; \\ \qquad S_M = 1,\ S_m = 0 \end{cases} \tag{25}$$

Focused on diode rectifiers, the DC voltage on output side u_{dc}(V) can be calculated as equation (26). As diode is on the state of cutting off, all diodes in paths shown in Fig. 7 cannot form a loop of ZCSS. As is shown in the equivalent circuit, the conditions that no ZSCC exists are shown in equation (27) and can be simplified as (28) further, where U_m (V) is the amplitude of phase voltage.

$$u_{dc} = \frac{3\sqrt{6}}{\pi} \times \frac{U_m}{\sqrt{2}} \tag{26}$$

$$\begin{cases} \max\{u_a, u_b, u_c\} + \dfrac{S_a + S_b + S_c}{3} u_{dc} \le u_{dc} \\ u_{dc} - \min\{u_a, u_b, u_c\} - \dfrac{S_a + S_b + S_c}{3} u_{dc} \le u_{dc} \end{cases} \tag{27}$$

When the sum of switching function $S_\sum = S_a + S_b + S_c$ is 0 or 3, inequalities (28) would be transformed into $U_m \le 0$, which can never be satisfied. When $S_\sum$ is 1 or 2, inequalities (28) would be transformed into $U_m \le U_{dc}/3$, from which the range of modulation radio M can be obtained shown as equation (29), which will limit the amplitude of the output voltage.

$$\begin{cases} U_m \le (1 - \dfrac{S_\sum}{3})u_{dc} \\ -U_m \ge -\dfrac{S_\sum}{3} u_{dc} \end{cases} \tag{28}$$

$$M = \frac{U_m}{\frac{\pi}{2} u_{dc}} \le \frac{\pi}{6} \tag{29}$$

On one hand, the modulation methods to eliminate ZCSS suffer the low utilization of DC link voltage with the maximum value of $\pi/6$; On the other hand, the switching states with $S_\sum = 0, 3$ are inevitable [35], [36]. Thus, a 3-phase inverter can inject power to the grid with a both step-up and isolated transformer, to block the inevitable ZCSS paths. As the drawbacks of line-frequency transformers mentioned in section I, an isolated DC/DC converter will be applied in shunt with the diode rectifier so that loops of ZCSS between the 3-phase inverter and the diode rectifier do not exist. Although the DC input side of the 3-phase inverter and that of the diode rectifier are not directly connected, the ZCSS has a short circuit path on the side of HFPET. At the same time, the application of HFPET separates the AC and the DC sides, improving reliability of shunt system.

IV. TOPOLOGY AND CONTROL OF THE PROPOSED ISOLATED APF AND CONTROL STRATEGY

The shunt isolated topology is composed of an LLC converter and a 3-phase inverter shown in Fig. 9, in which 4 switching

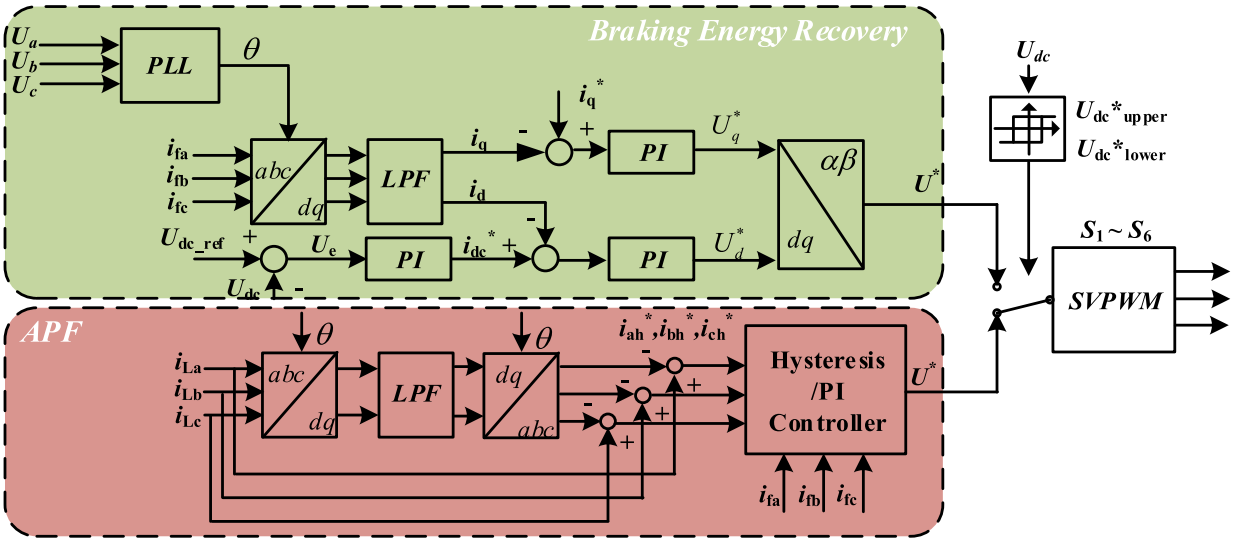

FIGURE 10. Closed-loop control strategy of APF and braking energy recovery.

devices are applied on the primary side of the LLC converter and 4 diodes are on the secondary side, so that single direction of power flow is ensured. $Q_1 \sim Q_4$ operate in switching mode with fixed switching frequency while energy flow of isolated converter is decided by the voltage relationship between two sides of HFPET. Operating states of switches in same bridge are compensated to avoid short current. As the output and input voltage of the converter are 1,180 V AC and 1,500 V DC respectively, the voltage gain of the LLC converter is designed as 1.2 to guarantee the function of APF, achieving ZCS and ZVS with switching frequency lower than the resonant frequency. The reference directions of load current both in primary and secondary sides of HFPET are also shown.

When powering trains, the diode rectifier is on the state of conducting, which acts as a typical non-linear load. Under this condition, harmonics should be compensated well with no braking energy recovery. In the process of braking, power flows from the traction grids to the city grids, and the voltage of the traction grid rises up and the diode rectifier does not conduct. In this case, non-linear characteristics of load no longer exist. The converter mainly acts as controlling current injecting into the 3-phase grid in higher quality.

Based on the above analysis in two different modes, the control strategy adopts double loops of voltage and current together with harmonics elimination, which is shown in Fig. 10. For PI controller, it can achieve controlling for direct value. But i_{fa}(A), i_{fb}(A), i_{fc}(A) and i_{La}(A),i_{Lb}(A),i_{Lc}(A) shown in Fig. 10 are all alternating currents which cannot be processed directly. In hence, Clarke and Park transformation are used to change static coordinate into rotating coordinate. Alternating values can be transformed into i_α, i_β and finally i_d, i_q by coordinate transformation matrix so that parameters can be processed by PI controller and close-loop control can be achieved. For harmonic elimination, harmonic components are detected from currents of

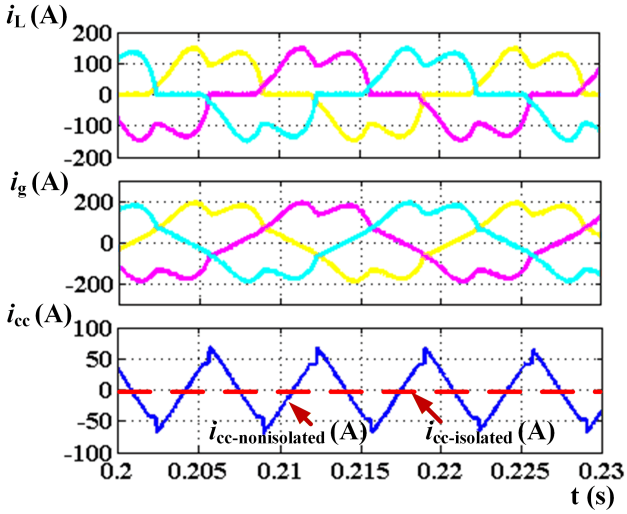

FIGURE 11. Load current i_L(A), grid current i_g(A) and circulating current i_{cc}(A). ZSCC of shunt APF directly connected to 3-phase grid without HFPET $i_{cc-nonisolated}$ (A) and ZSCC of shunt isolated APF with HFPET $i_{cc-isolated}$ (A).

the non-linear load i_{La}(A),i_{Lb}(A),i_{Lc}(A) after transformation of coordinates and low-pass filters. By PI controllers or hysteresis controllers, corresponding harmonic component i^*_{ah}(A), i^*_{bh}(A), i^*_{ch}(A) are generated by the APF so that the current on the grid side will be smoothed [37], [38]. When the converter operates in APF mode, PI and hysteresis controller can both achieve the objective of controlling separately. PI controller is based on triangular wave comparing method and switching frequency is constant. For the hysteresis controller, although hardware design and control strategy is simple, switching frequency is variable which puts up higher requirement for switching devices. During the braking process, when the voltage of DC bus U_{dc}(V) rises up to $U^*_{dc\ upper}$(V), the converter will act as a feedback converter in which PI controllers

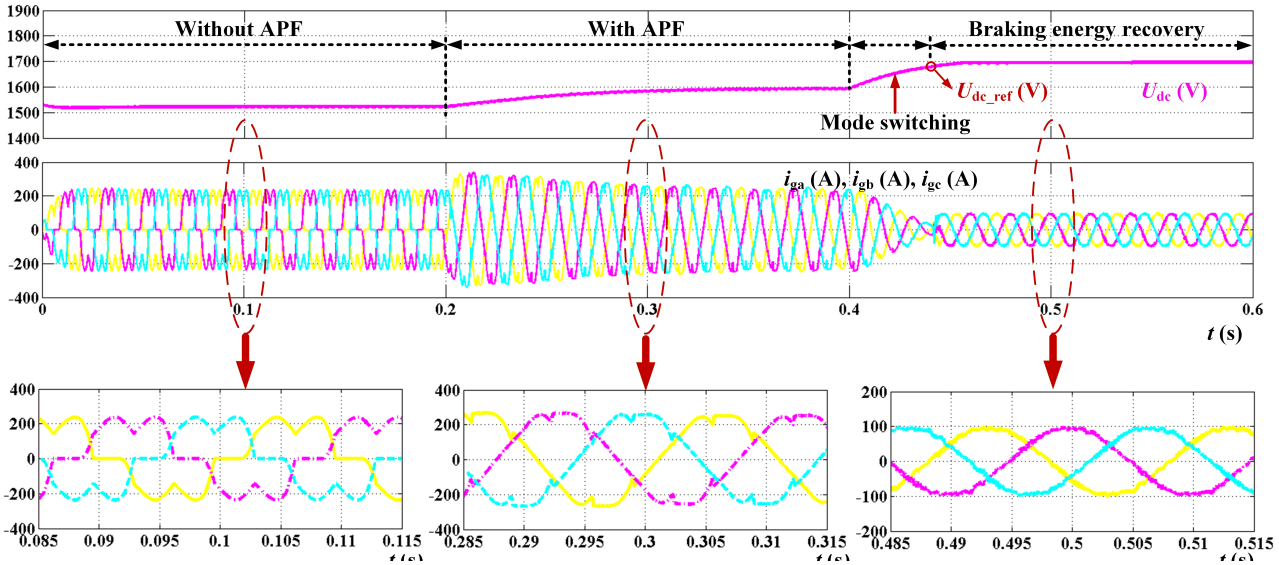

FIGURE 12. Simulation results of current on side of grid i_{ga}(A), i_{gb}(A), i_{gc} (A) and voltage of DC traction grid U_{dc} (V) under periods of without APF (running process of train), with APF (running process of train), mode switching period and braking energy recovery.

TABLE 4. Parameters Of The Shunt Topology Simulation.

Symbol	Quantity	Parameters
C_r	Series resonant capacitor	4.5 μF
L_r	Resonant inductance	10 μH
L_m	Magnetic inductance	0.1 mH
N	Turn radio of the HFPET	1: 1.2
L_a, L_b, L_c	Connecting grid inductance	5 mH
C_{dc}	Filter capacitor on DC side	820 μF
f_s	Switching frequency	10 kHz

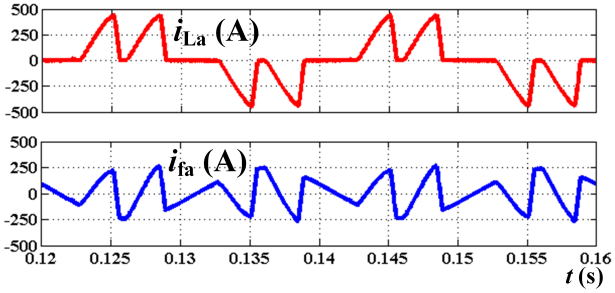

FIGURE 13. Simulation waves of non-linear load current i_{La}(A) and feedback current i_{fa} (A).

are applied to make feedback current i_{fa}(A), i_{fb}(A), i_{fc}(A) sinusoidal. During the traction process, when U_{dc}(V) drops to $U^*_{dc\ lower}$(V), APF mode of converter operates to eliminate harmonics. Mode switch is realized by hysteresis controller by software.

V. SIMULATION VERIFICATION

Simulation was done based on MATLAB/Simulink and PLECS. The parameters of simulation module are listed in table 4. If the shunt APF was directly connected to the 3-phase grid without the isolated step-up transformer, the ZCSS existed with a value of circulating current i_{cc} (A) which takes a part of load current i_{La} (A). Consequently, the ZCSS should be eliminated in order to increase safety and efficiency of the system by adding an isolated HFPET. On contrary, the ZSCC of isolated DC/DC converter was eliminated using the proposed converter in Fig. 11, in which $i_{cc-isolated}$(A) and $i_{cc-nonisolated}$(A) are ZSCC of isolated topology and non-isolated topology. Peak value of ZSCC in non-isolated topology $i_{cc-nonisolated}$(A) is 49.3 A which is 24% of grid current i_g(A). In hence, shunt isolated topology is verified.

Considering of simulation model on a shunt isolated APF with common DC link, a controlled current source was used to represent the train load which can absorb and generate power. During the whole process of train running and braking, currents on side of grid i_{ga}(A), i_{gb}(A), i_{gc}(A) and voltage of DC traction grid U_{dc}(V) are shown in Fig. 12, in which reference voltage U_{dc_ref} (V) is used to control the switching of mode. The functions of APF and braking energy recovery were both well achieved. Simulation waves of non-linear load current i_{La} (A) and feedback current i_{fa} (A) are shown in Fig. 13, which shows APF can generate harmonics for compensation. The FFT analysis of three processes are compared in Fig. 14 using a log scale (dB) in the y-axis. The THD of periods without APF, those with APFs and braking energy recovery were 28.44%, 7.22% and 5.43% respectively.

During the process of running and braking, function of DC link support and soft-switching of the LLC converter were both kept, which are shown in Fig. 15 respectively and i_{LLC} (A) is resonant current.

VI. EXPERIMENTAL VERIFICATION

The experimental setup (Fig. 16) consists a 1-kW prototype built in the lab. The parameters of devices and electrical

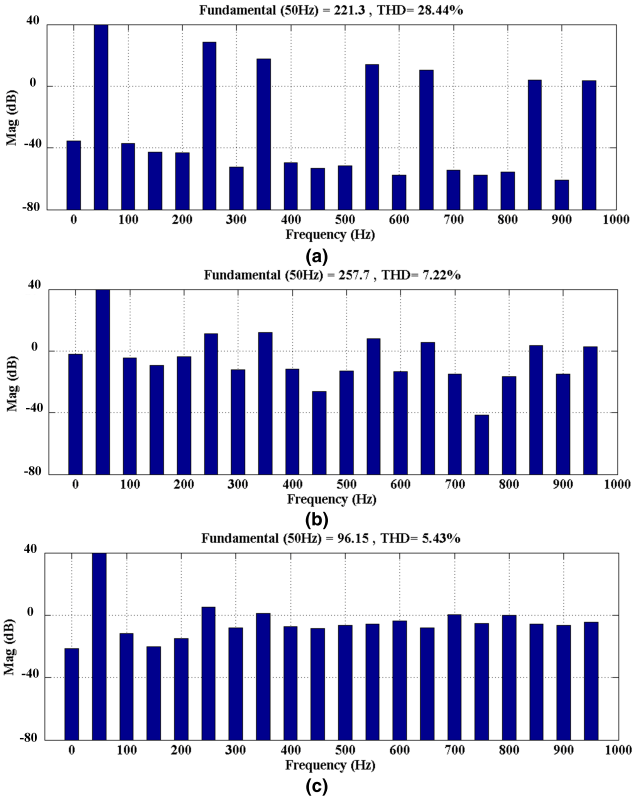

FIGURE 14. FFT analysis of i_{ga}(A) in three processes under periods of (a) without APF (running process of train), (b) with APF (running process of train) and (c) braking energy recovery.

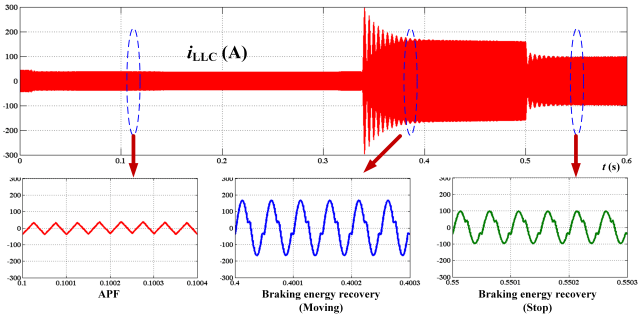

FIGURE 15. Simulation results of resonant current i_{LLC} (A) in shunt isolated converter during APF, braking energy recovery (Moving) and braking energy recovery (Stop).

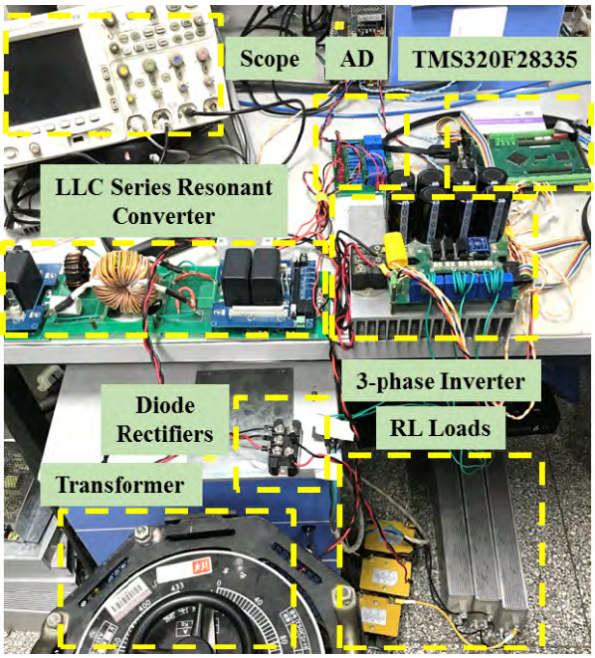

FIGURE 16. Picture of experiment platform of shunt isolated topology of LLC series resonant converter and 3-phase inverter.

TABLE 5. Parameters of the devices in experiment setup.

Symbol	Quantity	Parameters
C_{dc}	Capacitor connected to DC bus	200 uF (4 × 50 uF)
DRs	3-phase diode rectifiers	SanRex: MDS100A1600V
L_r	Resonant inductance	10 uH
C_r	Resonant capacitor	4.5 uF, mkp
L_c	Inductance connected to grid	2 mH

TABLE 6. Electrical parameters of HFPET design.

Symbol	Quantity	Parameters
$U_{in\text{-}max}$, $U_{out\text{-}max}$	Maximum input & output voltage of HFPET	500 V
$I_{in\text{-}max}$, $I_{out\text{-}max}$	Maximum input & output current of HFPET	10 A
N	Ratio of primary side and secondary side	1: 1.2
L_m	Magnetic inductance	7 mH
L_L	Leakage Inductance	10 uH

parameters of HFPET are shown in TABLE 5 and TABLE 6 respectively. The control strategy was implemented based on TMS320F28335 and CPLD EPM1270T144C5. The DSP achieved the closed-loop control while the CPLD was in charge of the LLC converter. An proposed DC/DC isolated converter is shown in Fig. 17.

The diode rectifiers (SanRex: MDS100A1600V) brought large amounts of harmonics and voltage distortion to the 3-phase grid. By shunt isolated APF with common DC link, compensation current is injected to grid to make current of all load sinusoidal. Results are shown in Fig. 18, in which i_{La} (A), i_{fa} (A) and i_{ga} (A) are current of diode rectifier, compensation current and current injected to grid respectively. FFT analysis has been done for i_{La} (A) and i_{ga} (A). THDs of i_{La} (A) and i_{ga} (A) are 23.07% and 12.98% respectively so that APF has taken effects, which are shown in Fig. 19 using a log scale (dB) in the y-axis. By comparison between isolated and shunt non-isolated topology, circulating current of shunt topology is shown in non-isolated converter while isolated DC/DC converter has an effective suppression of circulating current, which is shown in Fig. 20. $i_{cc-nonisolated}$ (A) is circulating current of non-isolated topology and $i_{cc-isolated}$ (A) is circulating current of shunt isolated topology. Peak value of circulating current is 1.78 A which is 23% of compensation current which is in accordance with the simulation result shown in section V.

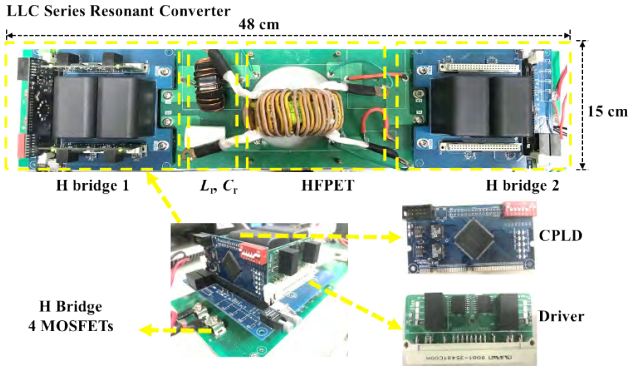

FIGURE 17. Experimental setup of LLC series resonant converter.

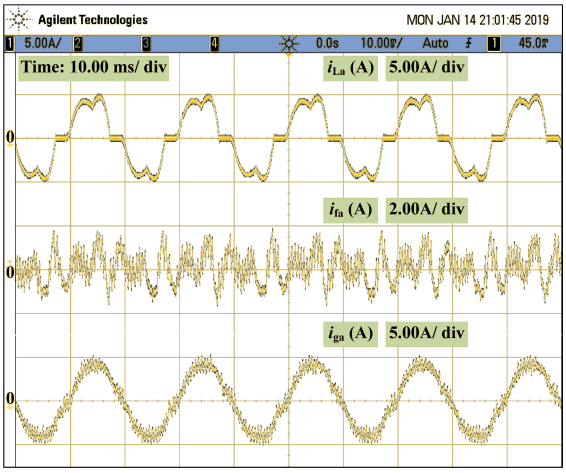

FIGURE 18. Experimental waves of isolated APF. Current of diode rectifier i_{La}(5 A/div), compensation current i_{fa}(2 A/div), and current injected to grid i_{ga}(5 A/div).

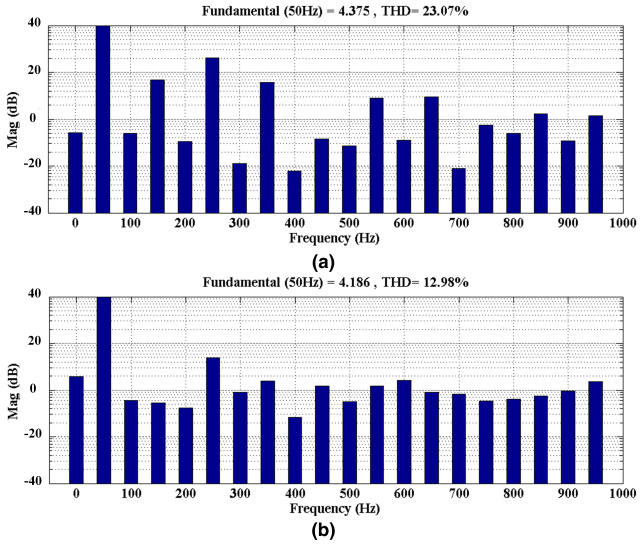

FIGURE 19. FFT analysis of experimental waves. (a) FFT analysis on current of diode rectifier i_{La} (A) (b) FFT analysis on current after compensation i_{ga} (A).

During the process of energy feedback when voltage of DC link rises up to reference value, shunt isolated converter realize power transmission from DC to AC together with

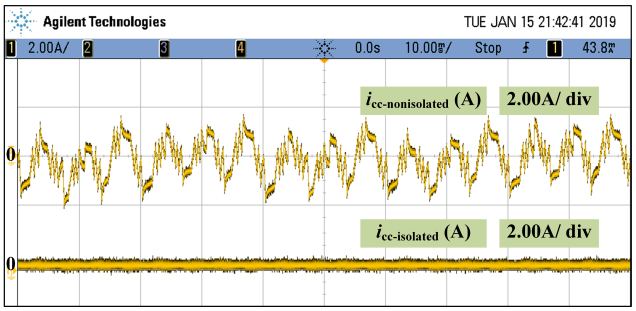

FIGURE 20. Experimental waves of circulating current. Circulating current of non-isolated topology $i_{cc-nonisolated}$ (2 A/div) and circulating current of isolated topology $i_{cc-isolated}$ (2 A/div).

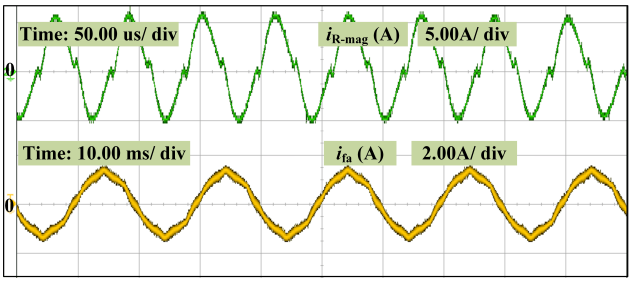

FIGURE 21. Experimental waves of energy feedback. Current of LLC converter in part i_{R-mag}(5 A/div) and feedback current i_{fa}(2 A/div).

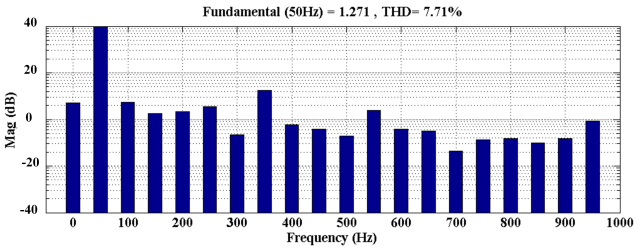

FIGURE 22. FFT analysis on feedback current i_{fa} (A).

soft-switching of LLC converter which is shown in Fig. 21. i_{R-mag} (A) is current of LLC converter and i_{fa} (A) is feedback current, harmonics of which is 7.71% by FFT analysis, which is shown in Fig. 22 using a log scale (dB) in the y-axis.

From the results of experiment, both APF and braking energy recovery are realized in lab environment. The switchover between two periods is decided by voltage of DC link.

VII. CONCLUSION

In urban rail transit, harmonics need to be suppressed and braking energy also should be utilized to reduce losses. In this paper, focuses on the problems of harmonics in urban rail transit while braking energy recovery is also included. Based on traditional shunt non-isolated APFs, it is shown that ZCSS would occur without an isolated HFPET, the amplitude of which is 23% of the load current which brings high losses and increases current stress of the switches. Two types of potential loops of ZCSS are analyzed and equivalent circuits are built for accurate analysis, which shows that the modulation radio

of the inverter would be constrained at the upper limit of $\pi/6$ to guarantee no ZSCC. Consequently, a shunt isolated APF with a common DC link integrating braking energy recovery is put forward to realize suppression of harmonics and elimination of ZSCC together with energy feedback. In this topology, the LLC series resonant converter operates in soft-switching condition of ZVS and ZCS, bringing high efficiency and wide voltage range. Closed-loop control strategy of voltage and current during period of APFs and braking energy recovery are designed respectively. During the process of starting and running of the train, the voltage of the DC bus is lower than the reference voltage, the converter is operating as the APF without ZSCC. In the process of braking, the voltage of the DC bus rises so that APF is paused and braking energy recovery is put into use. Simulation based on MATLAB/Simulink and PLECS has been done to verify analysis on characteristics of soft-switching and eliminating harmonics. A 1-kW prototype based on DSP and CPLD has been built to realize compensation of harmonics and energy feedback. All the needs are well satisfied and this novel converter combine two functions together and restrain ZCSS to realize an high DC voltage utilization with a smaller area and volume compared to traditional methods of achieving the APF and braking energy recovery.

REFERENCES

[1] W. Xu, "Comparisons and comments on harmonic standards IEC 1000-3-6 and IEEE Std. 519," in *Proc. 9th Int. Conf. Harmon. Qual. Power*, Orlando, FL, USA, Oct. 2000, pp. 260–263.

[2] M. Qasim, P. Kanjiya, and V. Khadkikar, "Optimal current harmonic extractor based on unified ADALINEs for shunt active power filters," *IEEE Trans. Power Electron.*, vol. 29, no. 12, pp. 6383–6393, Dec. 2014.

[3] P. H. Henning, H. D. Fuchs, A. D. L. Roux, and H. D. T. Mouton, "A 1.5-MW seven-cell series-stacked converter as an active power filter and regeneration converter for a DC traction substation," *IEEE Trans. Power Electron.*, vol. 23, no. 5, pp. 2230–2236, Sep. 2008.

[4] A. S. Lock, E. R. C. da Silva, M. E. Elbuluk, and D. A. Fernandes, "An APF-OCC strategy for common-mode current rejection," *IEEE Trans. Ind. Appl.*, vol. 52, no. 6, pp. 4935–4945, Dec. 2016.

[5] H. Hu, Z. He, and S. Gao, "Passive filter design for china high-speed railway with considering harmonic resonance and characteristic harmonics," *IEEE Trans. Power Del.*, vol. 30, no. 1, pp. 505–514, Feb. 2015.

[6] X. Du, L. Zhou, H. Lu, and H.-M. Tai, "DC link active power filter for three-phase diode rectifier," *IEEE Trans. Ind. Electron.*, vol. 59, no. 3, pp. 1430–1442, Mar. 2012.

[7] P. G. Barbosa, J. A. Santisteban, and E. H. Watanabe, "Shunt-series active power filter for rectifiers AC and DC sides," *IEE Proc. Electr. Power Appl.*, vol. 145, no. 6, pp. 577–584, Nov. 1998.

[8] B. Zhao, S. Qiang, W. Liu, and Y. Sun, "Overview of dual-active-bridge isolated bidirectional DC-DC converter for high-frequency-link power-conversion system," *IEEE Trans. Power Electron.*, vol. 29, no. 8, pp. 4091–4106, Aug. 2014.

[9] S. Rahmani, N. Mendalek, and K. Al-Haddad, "Experimental design of a nonlinear control technique for three-phase shunt active power filter," *IEEE Trans. Ind. Electron.*, vol. 57, no. 10, pp. 3364–3375, Oct. 2010.

[10] M. Habibullin, V. Pikalov, V. Mescheryakov, and S. Valtchev, "Active power filter with common DC link for compensation of harmonic distortion in power grids," in *Proc. 16th Int. Power Electron. Motion Control Conf. Exposit.*, Sep. 2014, pp. 1345–1349.

[11] Z. Ye, D. Boroyevich, J.-Y. Choi, and F. C. Lee, "Control of circulating current in two parallel three-phase boost rectifiers," in *Proc. 15th Annu. IEEE Appl. Power Electron. Conf. Exposit.*, New Orleans, LA, USA, Sep. 2000, pp. 506–512.

[12] D. Zhang, F. F. Wang, R. Burgos, and D. Boroyevich, "Common-mode circulating current control of paralleled interleaved three-phase two-level voltage-source converters with discontinuous space-vector modulation," *IEEE Trans. Power Electron.*, vol. 26, no. 12, pp. 3925–3935, Dec. 2011.

[13] N. M. L. Tan, T. Abe, and H. Akagi, "Design and performance of a bidirectional isolated DC-DC converter for a battery energy storage system," *IEEE Trans. Power Electron.*, vol. 27, no. 3, pp. 1237–1248, Mar. 2012.

[14] B. Zhao, Q. Song, and W. Liu, "Efficiency characterization and optimization of isolated bidirectional DC-DC converter based on dual-phase-shift control for DC distribution application," *IEEE Trans. Power Electron.*, vol. 28, no. 4, pp. 1711–1727, Apr. 2013.

[15] H. Xu, Z. Yin, Y. Zhao, and Y. Huang, "Accurate design of high-efficiency LLC resonant converter with wide output voltage," *IEEE Access*, vol. 5, pp. 26653–26665, Sep. 2017.

[16] J.-H. Jung, H.-S. Kim, M.-H. Ryu, and J.-W. Baek, "Design methodology of bidirectional CLLC resonant converter for high-frequency isolation of DC distribution systems," *IEEE Trans. Power Electron.*, vol. 28, no. 4, pp. 1741–1755, Apr. 2013.

[17] C. Liu, H. Liu, G. Cai, S. Cui, H. Liu, and H. Yao, "Novel hybrid LLC resonant and DAB linear DC-DC converter: Average model and experimental verification," *IEEE Trans. Ind. Electron.*, vol. 64, no. 9, pp. 6970–6978, Sep. 2017.

[18] F. Lin, "Control strategies with dynamic threshold adjustment for supercapacitor energy storage system considering the train and substation characteristics in urban rail transit," *Energies*, vol. 9, no. 4, p. 257, 2016.

[19] L. Yutong, Z. Xiaohao, and Z. Yehui, "Application of regenerative braking energy absorption devices in beijing subway," *Urban Rapid Rail Transit*, vol. 27, no. 4, pp. 105–108, 2014.

[20] M. Ogasa, "Energy saving and environmental measures in railway technologies: Example with hybrid electric railway vehicles," *IEEE Trans. Elect. Electron. Eng.*. vol. 3, no. 1, pp. 15–20, May 2008.

[21] C. T. Pan and Y. H. Liao, "Modeling and coordinate control of circulating currents in parallel three-phase boost rectifiers," *IEEE Trans. Ind. Electron.*, vol. 54, no. 2, pp. 825–838, Apr. 2007.

[22] C. T. Pan and Y. H. Liao, "Modeling and control of circulating currents for parallel three-phase boost rectifiers with different load sharing," *IEEE Trans. Ind. Electron.*, vol. 55, no. 7, pp. 2776–2785, Jul. 2008.

[23] X. Liu, E. Lei, X. Yin, J. Wang, and M. Wen, "A cooperative control strategy of energy storage system and inverter for regenerative braking energy," in *Proc. 11th World Congr. Intell. Control Automat.*, Jul. 2014, pp. 2985–2990.

[24] S. Ding, "Application of braking energy recovery," in *The Principle Energy Feedback Traction Power Supply Its Application Urban Rail Transit*, 1th ed. Beijing, China: BJTU, 2014, pp. 229–232.

[25] L. Wang, G. Zhang, M. Shen, H. Quan, and Z. Liu, "A novel traction supply system for urban rail transportation with bidirectional power flow and based on PWM rectifier," in *Proc. Int. Conf. Energy Environ. Technol.*, Guilin, Guangxi, China, Oct. 2009, pp. 40–43.

[26] X. Lu, Z. Liu, L. Wang, and M. Shen, "On the characteristics of a novel traction power supply system based on three-level voltage-source PWM rectifier," in *Proc. IEEE Vehicle Power Propuls. Conf.*, Sep. 2008, pp. 1–4.

[27] V. Gelman, "Insulated-gate bipolar transistor rectifiers: Why they are not used in traction power substations," *IEEE Veh. Technol. Mag.*, vol. 9, no. 3, pp. 86–93, Sep. 2014.

[28] S. Bernet, "Recent developments of high power converters for industry and traction applications," *IEEE Trans. Power Electron.*, vol. 15, no. 6, pp. 1102–1117, Nov. 2000.

[29] M. Popescu, A. Bitoleanu, and A. Preda, "A new design method of anLCLFilter applied in active DC-traction substations," *IEEE Trans. Ind. Appl.*, vol. 54, no. 4, pp. 3497–3507, Jul./Aug. 2018.

[30] L. Hao, Z. Zedong, D. Qin, and X. Zheng, "A novel urban rail transit system based on DC distribution and energy internet architecture," in *Proc. IEEE Conf. Energy Internet Energy Syst. Integr.*, Nov. 2017, pp. 1–6.

[31] L. B. Perera, N. R. Watson, Y. H. Liu, and J. Arrillaga, "Multilevel current reinjection self-commutated HVDC converter," *IEE Proc. Gener., Transmiss. Distrib.*, vol. 152, no. 5, pp. 607–615, Sep. 2005.

[32] G. Carpinelli, F. Iacovone, A. Russo, P. Varilone, and P. Verde, "Analytical modeling for harmonic analysis of line current of VSI-fed drives," *IEEE Trans. Power Del.*, vol. 19, no. 3, pp. 1212–1224, Jul. 2004.

[33] Z. Yang, Z. Yang, F. Lin, H. Xia, and X. Li, "Adjustment of metro train operation curve for efficiently using regenerative energy," in *Proc. 42nd Annu. Conf. IEEE Ind. Electron. Soc.*, Oct. 2016, pp. 3806–3811.

[34] M. Pena-Alcaraz, "Optimal underground timetable design based on power flow for maximizing the use of regenerative-braking energy," *Inst. Mech. Engineers F, J. Rail Rapid Transit*, vol. 226, no. 4, pp. 397–408, 2011.
[35] G. Li, Z. Zheng, Y. Li, and Z. Wang, "Synchronous SVPWM over-modulation method based on zero-sequence voltage injection in locomotive traction," in *Proc. 18th Eur. Conf. Power Electron. Appl.*, Sep. 2016, pp. 1–10.
[36] G. Li, Y. Li, M. Tang, Y. Li, and Z. Zheng, "Rotror flux-oriented control of PMSM with synchronized carrier SVPWM and zero sequence voltage injection over-modulation for traction application in very low switching frequency," in *Proc. IEEE 3rd Int. Future Energy Electron. Conf. ECCE Asia* , Jun. 2017, pp. 1634–1640.
[37] Z. Shuquan, "Selective harmonic current control based on multiple synchronous rotating coordinates," in *Proc. CSEE*, May 2010, pp. 55–62.
[38] T. Xin, L. An, and T. Chunming, "Recursive integral PI for current control of hybrid active power filter," in *Proc. CSEE*, vol. 23, no. 10, May 2003, pp. 38–41.

HAO LIU (S'17) was born in Shandong, China, in 1994. He received the B.S. degree in electrical engineering from the Department of Electrical Engineering, Tsinghua University, Beijing, China, in 2016, where he is currently pursuing the master's degree.

His current research interests include urban rail transit, power electronics transformer, and the energy internet.

CHI LI (S'14–M'18) received the B.S. degree in electrical engineering from Tsinghua University, Beijing, China, in 2012, and the M.S. and Ph.D. degrees in electrical engineering from Virginia Tech, Blacksburg, VA, USA, in 2015 and 2018, respectively.

From 2012 to 2018, he was a Research Assistant with the Center for Power Electronics Systems (CPES), Virginia Tech. In 2018, he returned to Tsinghua University, where he is currently a Postdoctoral Researcher with the Department of Electrical Engineering. His research interest includes control and stability of power electronics converters and systems.

ZEDONG ZHENG (M'09) was born in Shandong, China, in 1980. He received the B.S. and Ph.D. degrees in electrical engineering from Tsinghua University, Beijing, China, in 2003 and 2008, respectively.

He is currently a Faculty Member with the Department of Electrical Engineering, Tsinghua University. His research interests include power electronics converters and high-performance motor control systems.

JIYE LIU (S'18) was born in Hebei, China, in 1993. He received the B.S. degree in electrical engineering from the Department of Electrical Engineering, Tsinghua University, Beijing, China, in 2017, where he is currently pursuing the Ph.D. degree.

His current research interests include multilevel converters, power electronic transformers, and the control of power converters.

YONGDONG LI (M'08) was born in Hebei, China, in 1962. He received the B.S. degree from the Harbin Institute of Technology, China, in 1982, and the M.S. and Ph.D. degrees from the Department of Electrical Engineering, Institute National Polytechnique de Toulouse, Toulouse, France, in 1984 and 1987, respectively, all in electrical engineering.

Since 1996, he has been a Professor with the Department of Electrical Engineering, Tsinghua University, Beijing, China. His research interests include power electronics, machine control, and wind power generation.